ELSEVIER
SAUNDERS

Radiol Clin N Am 42 (2004) 1017 – 1032

RADIOLOGIC
CLINICS
of North America

PET/CT scanner instrumentation, challenges, and solutions

Adam M. Alessio, PhD[a], Paul E. Kinahan, PhD[a,*], Phillip M. Cheng, MD[a], Hubert Vesselle, MD, PhD[a], Joel S. Karp, PhD[b]

[a]*Department of Radiology, University of Washington, 1959 NE Pacific Street, Box 356004, Seattle, WA 98195–6004, USA*
[b]*Department of Radiology, University of Pennsylvania, 3400 Spruce Street, 110 Donner Building, Philadelphia, PA 19104, USA*

PET radiotracer imaging with the labeled glucose analogue [^{18}F]-fluorodeoxyglucose (FDG) is increasingly being used in oncology imaging because of its usefulness in detecting and staging cancer and metastatic disease [1–4]. For most clinical or research applications of PET, functional measurements of radiotracer uptake require PET images of diagnostic quality together with correlative anatomic imaging to permit optimal interpretation of this uptake. In particular, in the clinical setting of an FDG-PET scan performed for initial tumor staging, the clinical significance of a given focus of increased FDG uptake depends on the location of the focus, the type of tumor staged, the multiplicity of uptake foci, and the therapeutic options available for the patient. FDG-PET scans often require a recently performed anatomic imaging study for correlation and final PET interpretation. A CT examination is the most common such anatomic imaging study acquired. Visual coregistration of FDG-PET and CT is then performed to reach a final diagnosis with the morphology of a lesion on CT adding further to the specificity of the reading. In some instances, however, the time interval between CT and PET examinations or the inability perfectly to co-register the two prevents optimal interpretation.

Software registration techniques can provide more accurate localization than achievable with visual coregistration of separate anatomic and functional images. The software registration field offers a host of advanced algorithms for aligning two scans [5,6]. These algorithms range from simple scaling methods to dynamic transformations based on mutual information in the images [7] and other methods. Software registration has been proved to work well for rigid body applications, such as brain imaging [8]. Whole-body studies, however, in which deformable organs change in shape and location because of variable inspiration and patient movement, require nonrigid registration algorithms that are prone to errors especially at boundaries [9]. Erroneous registrations force transformations on the PET image that could lead to errors in disease localization and diagnosis. For example, the clinical significance of a focus of FDG uptake changes greatly when it is mapped to the mediastinum instead of the adjacent lung parenchyma. Similarly, a focus of FDG uptake is interpreted differently if localized to the chest wall or the adjacent lung periphery. Software registration of separate scans must overcome challenges varying in complexity from different image sizes to disease progression between scans taken at significantly different times. In addition, there has been no systematic validation of any nonrigid registration method, unlike the use of the Vanderbilt PET/CT-MR imaging brain data set [8] for testing rigid registration methods.

An alternative to software registration is a single device with both functional and anatomic capacities. This device, through its shared mechanical compo-

This work was supported by National Institutes of Health Grant CA-74135.

* Corresponding author.
E-mail address: kinahan@u.washington.edu (P.E. Kinahan).

0033-8389/04/$ – see front matter
doi:10.1016/j.rcl.2004.08.001

nents, provides a straightforward hardware solution to the alignment of anatomic and functional images. One of the original combined devices was a CT and single-photon emission CT system developed by Lang et al in 1992 [10]. Although their original system was fully integrated with shared electronics and detectors, their design evolved into a combination of independent CT and single photon emission CT devices to improve performance. The first PET/CT scanner was introduced in 1998 through a collaboration of the National Cancer Institute, CTI PET Systems (Knoxville, Tennessee), and the University of Pittsburgh [11]. This scanner was constructed from independent, previously developed CT and PET scanners. The combination of independent components remains the standard for scanner design today.

PET/CT scanners provide a simple solution to the localization task. Fig. 1 presents a PET/CT scan with the separate PET (Fig. 1A) and CT (Fig. 1B) sagittal images of the head and the combined PET/CT image (Fig. 1C). This hardware alignment of the images reveals that a tumor is located in the right retropharyngeal space, an interpretation difficult to make on the basis of a CT alone.

Along with offering an aligned functional and anatomic image, the CT component can supply information for PET attenuation correction. Conventional PET scans require a lengthy transmission scan to perform attenuation correction of the emission data for accurate radiotracer uptake quantitation. The attenuation image from the CT provides a fast, noise-free alternative thereby significantly reducing overall scan time and noise contributions from the transmission scan.

Although the clinical role of PET/CT has not been clearly defined, an increasing number of clinical studies have explored the application of PET/CT in cancer diagnosis, staging, and prognosis. The scope of these PET/CT studies encompasses tumors of the

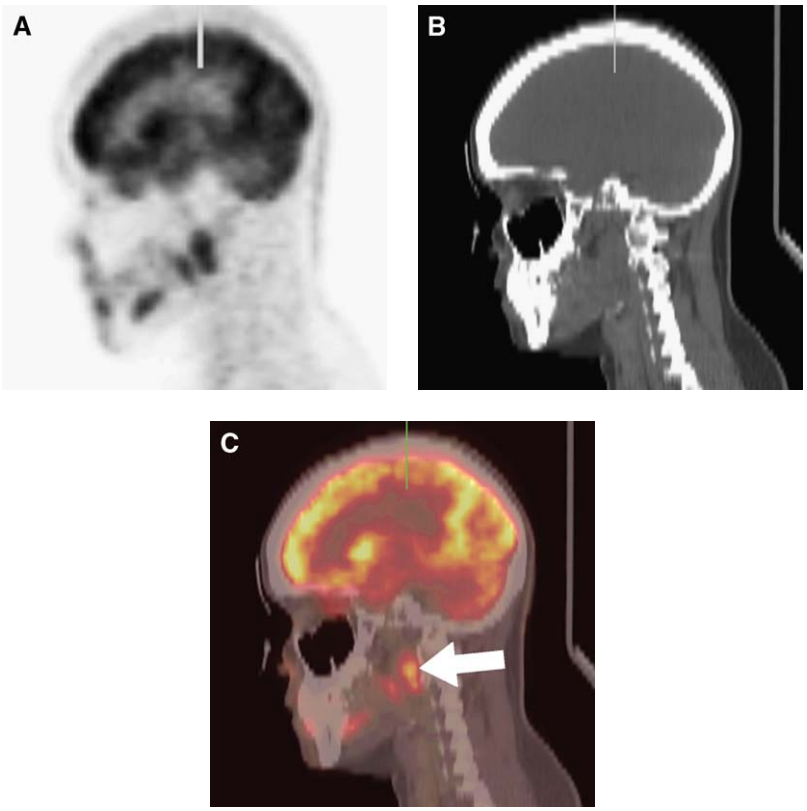

Fig. 1. Example of tumor localization and hardware image alignment using a PET/CT scanner. (*A*) Sagittal PET image, (*B*) sagittal reformatted CT image, and (*C*) PET/CT image with CT component in gray scale and PET image in red temperature color scale. The PET/CT image reveals tumor localization in the right retropharyngeal space (*arrow*).

head and neck [12–14], thyroid [15], lung [13,16], gastrointestinal tract [17–19], pelvis [19–21], and spine [22]. A recent study has reported improved reader confidence in discerning and localizing metabolic abnormalities, although with variable impact on staging accuracy and management [23]. Clearly, more evidence is needed to establish the appropriate clinical settings and expected benefits for diagnostic and staging PET/CT studies.

PET/CT is also finding potential value for radiation therapy planning. In particular, with recent advances in intensity-modulated radiation therapy, it is now possible to treat tumors while reducing radiation doses to nontarget organs compared with traditional techniques. This, however, requires precise delineation of target tissues. Although preliminary studies have explored the use of software-based image registration of PET and CT for radiation treatment planning [24,25], studies of PET/CT in radiation treatment planning remain in early feasibility stages [26].

This article focuses on PET/CT instrumentation, presenting a brief review of the current commercial PET/CT systems and discussing some of the benefits, major limitations, and future promise of this technology.

PET/CT scanner design

In a broad sense, a PET/CT scanner consists of three main components: (1) a PET scanner, (2) a CT scanner, and (3) a patient bed. Currently, all of the major commercial systems consist of a PET component with independent detectors, electronics, and acquisition system, and a CT component with its own set of independent modules. Because the main impetus for a combined system lies in the ability to understand functional activity better, there remains some debate about the required CT imaging capabilities on these systems. Currently, vendors offer many options for the CT component including 2- through 16-slice systems.

A drawing highlighting the major components of a typical PET/CT scanner appears in Fig. 2. A single bed moves axially into the scanner while the patient receives first a CT scan and then a PET scan. Even though many of the design challenges in this scanner, such as gantry rotation and data collection, have already been solved in their independent scanner technologies, this combined system presented several new challenges. For instance, the patient bed needed to be redesigned to reduce vertical deflection as it traveled into the axial field of view. Because the original CT or PET beds would have resulted in serious vertical misalignment between the scans, each vendor developed unique patient handling systems for their PET/CT scanner. Another nontrivial challenge lies in the need to service the scanner modules, each of which needs to be accessed from both sides.

Table 1 provides some key specifications for all of the current, commercial PET/CT systems. It should be stressed that these systems cannot be fully compared with the summarized listing presented here; a thorough understanding of the underlying influence of each parameter, such as the benefits of two-dimensional versus fully three-dimensional PET or different PET transmission modes, should be taken into account when comparing scanners. A discussion of two-dimensional versus fully three-dimensional is given elsewhere in this issue; transmission modes are discussed later.

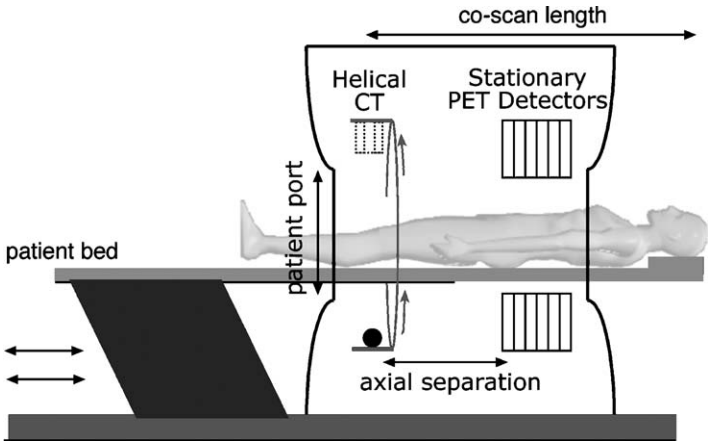

Fig. 2. Illustration of the major PET/CT scanner components.

Table 1
Key specifications for current commercial PET/CT scanners

	GEHS[a]		CPS		
	DLS	DST	PICO[b]	HIREZ[c]	Philips[d] Gemini
Scanner					
Patient port diameter (cm)	70 (CT) tapered to 59 (PET)	70	70	70	70 (CT) and 63 (PET)
Min room size (ft)	13.4 × 24	14 × 24	15 × 24.8	15 × 24.8	14 × 24
PET TX modes[e]	X-ray, 68Ge	X-ray	X-ray	X-ray	X-ray, 137Cs
Bed type	Double cantilever	Double cantilever	Fixed with sliding support	Fixed with sliding support	Single cantilever with center support
Coscan length (cm)	160/200	160	182	182	190
Max bed load (lbs)	400	400	450	450	430
PET component	Nxi	—	Wide-bore Accel	—	Wide-bore Allegro
Detector material	BGO	BGO	LSO	LSO	GSO
Acquisition mode	2D/3D	2D/3D	3D	3D	3D
Detectors per ring	672	420	384	624	616
Det ring diameter (cm)	92.7	88.6	83	83	90
Crystal dim (mm) trans × axial × thick	4.0 × 8.0 × 30	6.3 × 6.3 × 30	6.45 × 6.45 × 25	4.0 × 4.0 × 20	4.0 × 6.0 × 20
Number of rings	18	24	24	39	29
Transaxial FOV (cm)	55	70	58.5	58.5	57.6
Image planes	35 × 4.3	47 × 3.3	47 × 3.4	81 × 2.0	90 × 2.0
Axial FOV (cm)	15.2	15.7	16.2	16.2	18

CT component	Lightspeed		Lightspeed		Somatom		Somatom		Brilliance 16 or Mx8000 Dual	
Transaxial FOV	50		50		50		50		50	
Number of slices	4	8	8	16	2	16	6	16	2	16
Min slice thickness (mm)	0.63	0.63	0.63	0.625	1.0	0.6	1.0	0.6	0.5	0.6
Max slice col[e] (mm)	20	20	20	20	10	22.5	15	22.5	20	24
Min rotation time (s)	0.5	0.5	0.5	0.5	0.8	0.6	0.6	0.42	0.5	0.5
Max tube current (mA)	440	440	440	440	240	500	345	500	400	500

Abbreviations: FOV, field of view; TX, transmission; 2D, two-dimensional; 3D, three dimensional.

[a] General Electric Healthcare (www.gehealthcare.com) *Discovery* [*LS* and *ST*] are both offered with 4-, 8-, or 16- slice CT scanners.

[b] CPS *PICO* (www.cpspet.com) sold through CTI Molecular Imaging (www.ctimi.com) as the *Reveal* [*RT* or *XVI*] and through Siemens (www.medical.siemens.com) as the *Biograph 2*.

[c] CPS *HIREZ* sold through CTI as *Reveal* [*HiRez(6)* or *XVI HiRez*] and through Siemens as *Biograph* [*6* or *16*].

[d] Philips Medical Systems (www.medical.philips.com).

[e] Maximum slice collimation at isocenter.

Many PET/CT scanners have a patient port with a larger diameter than stand-alone PET systems. Conventionally, a CT scanner has a port with a diameter of 70 cm, whereas a dedicated PET scanner has a port diameter of 60 cm. Newer PET/CT scanners feature a port diameter of 70 cm to match the CT port facilitating the scanning of patients with the common CT protocol calling for arms positioned above the head (see Table 1; Fig. 3). The larger aperture also increases patient comfort. This wider port required the reduction of the detector module end shielding. Another design change for the PET component is the use of a smaller detector ring diameter than stand-alone PET systems to reduce external dimensions. During fully three-dimensional PET acquisition, the combined effect of the reduced end shielding and reduced detector ring diameter leads to a larger field of view for random and scattered coincidences (see Fig. 3). Even with accurate scatter and random coincidence corrections, the increased levels of these factors result in increased noise in the emission image.

In a typical PET/CT protocol, the operator initiates a whole-body scout CT scan (~2–10 s) to

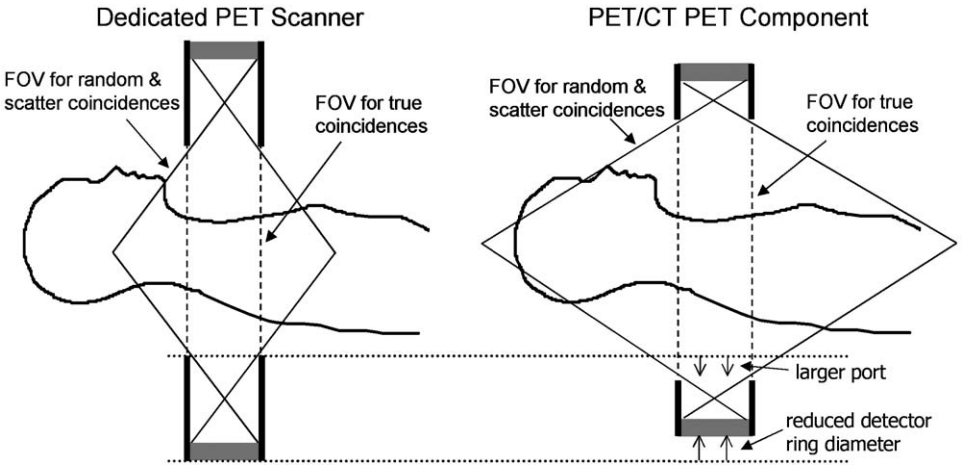

Fig. 3. Illustration of detector modules for dedicated PET scanner and PET/CT PET component operating in fully three-dimensional mode. The overall diameter of the patient port for the PET/CT PET component is typically greater. The PET/CT component also typically has a reduced detector ring diameter and shorter end shielding resulting in the undesirable behavior of accepting more random and scattered coincidences from outside the true coincidence field of view.

select a scan region. Then a whole-body, helical CT scan (~30 s–2 min) precedes the PET scan (approximately 5–45 minutes). Fig. 4 presents a flowchart of the major steps that occur from acquisition to image display. After acquisition, the CT processor corrects and reconstructs the CT data into an image. Then, to perform CT-based attenuation correction, the CT image is downsampled to PET resolution and translated (scaled with the bilinear or hybrid method discussed later) to 511-keV energies. The translated image is forward projected into the PET data format and used to correct the original PET emission data. These attenuation-corrected PET data are reconstructed on the PET processor. Finally, the images are overlaid and displayed on a shared console. There are several variations from this protocol using more sophisticated final image registration or attenuation-correction techniques. These variations are the topics of the next two sections.

Combined image display in PET/CT

The combination of anatomic and functional images is often called "fusion." It should be stressed that the images are never "fused" together and there is no DICOM mechanism for transferring aligned PET/CT images. The term "fusion" in this field often refers to the visualization of two distinct images on the same display and is probably better denoted as "merged." There are several methods for merging images on a single display [27] and a common

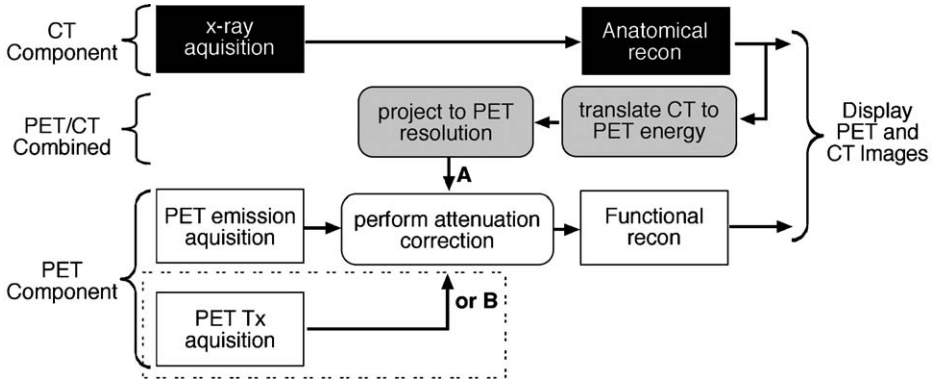

Fig. 4. Flow chart of a typical PET/CT operation. Attenuation correction factors can be obtained from either (*A*) CT-based or (*B*) conventional PET transmission source.

PET/CT method is "alpha" blending. In this method, the color display values in the PET image are averaged with those of the CT image and the contribution of the PET versus the CT in the final image can be varied with the alpha term, which ranges from $0 \leq \alpha \leq 1$. Also, side-by-side viewing of the PET emission and CT images with "locked cursors" is a useful technique because overlaying images causes a reduction in the CT contrast [27].

Despite strong benefits over software registration, PET/CT images can have alignment errors. Incorrect calibration of the PET/CT system, patient movement, and respiratory or cardiac motion can lead to alignment errors in the final images. A PET/CT system calibration requires accurate alignment of the CT gantry, PET gantry, and bed [28]. Currently, there are no standards for testing the alignment of PET/CT scanners. Patient movement during and between the CT and PET scans also remains a concern.

Along with errors from calibration and patient movement, PET/CT scans remain subject to errors from respiratory motion. The CT scan rapidly captures an image, often taken during full inspiration, and the PET scan captures an averaged respiratory cycle [29]. Several organs, especially the liver and spleen, experience deviations both in volume and position during respiration. Nakamoto et al [30] showed that when using a PET/CT protocol calling for no breathholds, the liver in the PET image is on average slightly larger (1%–7% larger in some dimensions) than the CT and the spleen is slightly smaller. As expected, the greatest respiratory deviations occur in the upper margin of the liver and lower margin of the spleen. Statistically, across many cases, these organ deviations between the scans are modest, but in individual cases these deviations could result in inaccurate localization. Choosing an optimal breathing protocol can help to reduce these deviations. Goerres et al [31] have shown that a breathhold at the end of a normal expiration (nonforced) during the CT scan and normal respiration during the PET scan can significantly reduce the respiratory errors found in several other conventional protocols. Given these possible alignment difficulties, registration algorithms may still have a role to play in a PET/CT scanner for small-scale rigid or nonrigid alignment.

CT-based attenuation correction

A brief review of CT-based attenuation correction for PET/CT scanners is provided next. For a more detailed description, readers are referred to the review article by Kinahan et al [32]. As photons travel through matter they can be absorbed or scattered. The combination of these interactions forces the attenuation of transmitted photons. This effect is often characterized by the linear attenuation coefficient μ, defined as the probability per unit path length that a photon undergoes photoelectric absorption or Compton scatter so that it is not detected.

The goal of CT imaging is to generate an attenuation map, whereas attenuation of the annihilation photons is a major source of error in PET imaging, if uncorrected. In PET, the matter in the body nonuniformly attenuates photons resulting in erroneous information about the actual quantity of radiotracer. Without corrections for this physical effect, PET images have quantitatively inaccurate activity concentrations with a spatial dependence. A thorough discussion of the ongoing debate regarding the need to perform attenuation correction is beyond the scope of this article [33,34].

Attenuation correction with PET/CT

To correct for the effects of attenuation, one needs to have knowledge of the linear attenuation coefficient for 511-keV photons along each line of response of the PET scanner. This knowledge can be obtained by performing a patient-specific transmission scan with an external source, similar in concept to a CT scan but at PET photon energies. Conventional PET scanners use either a ^{68}Ge-^{68}Ga rod sources of positrons for 511-keV annihilation photons or ^{137}Cs point sources of 662-keV single-photon gamma rays for acquiring a transmission scan, which can then be reconstructed as an attenuation image if desired for, say, noise suppression techniques (Fig. 5). The transmission scan is either then used directly or the reconstructed attenuation image is forward projected to provide attenuation correction factors for each PET line of response. Either approach uses the PET detectors for the data collection resulting in images with high levels of noise and low resolution compared with CT images. In addition, significant patient acquisition time is needed to collect sufficient photons to form a useable attenuation image. Using positron sources, common protocols often require approximately 3 to 7 minutes per bed position to form an attenuation image that is later segmented to reduce the noise. To form an adequate measured attenuation image (not requiring segmentation), one needs to do transmission scans of greater than 10 minutes per bed position depending on patient thickness (see Fig. 5 for a comparison of scan times). The time for a

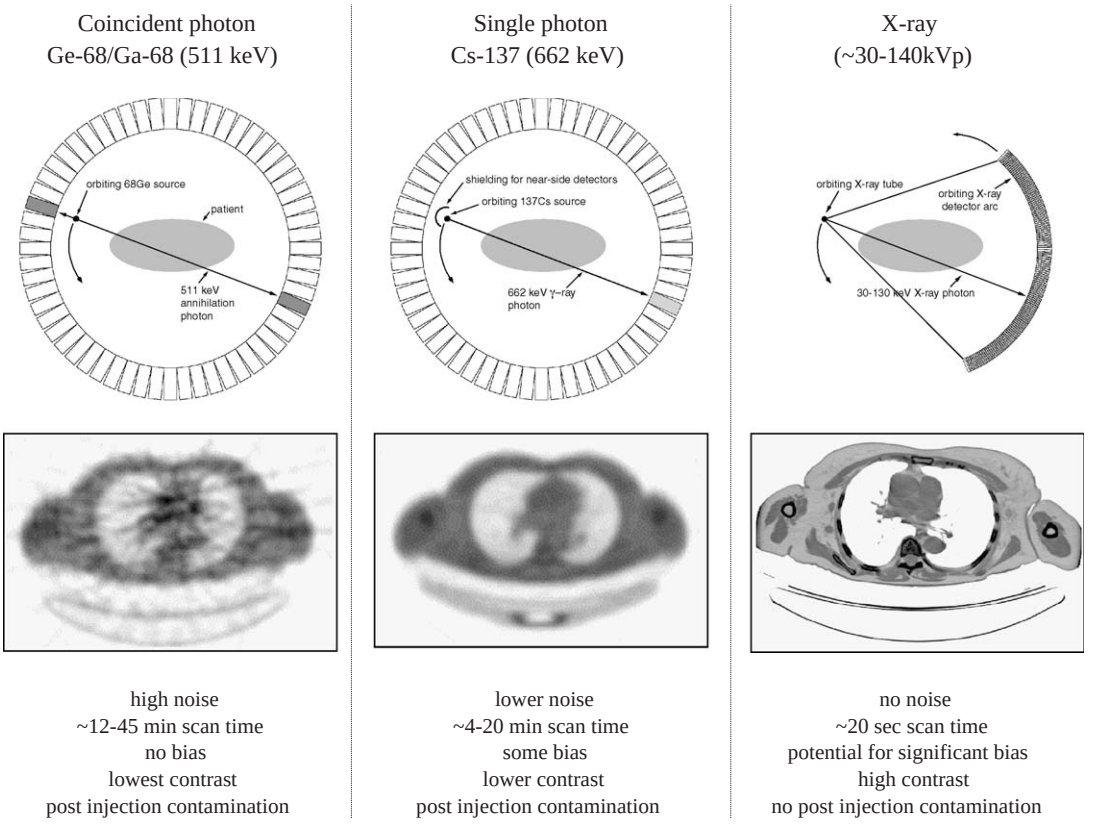

Fig. 5. Transmission scans used to collect attenuation information for PET attenuation-correction factors.

transmission image in a typical PET scan can represent as much as half of the total scan time [35].

With a PET/CT scanner, attenuation correction of the PET data can also be performed based on the CT transmission image (see Fig. 5). CT scans are orders of magnitude faster than PET transmission scans. This time reduction represents a significant benefit both in the overall throughput ability of a scanner and in patient comfort. Furthermore, CT images are virtually noise free and unaffected by emission photons. For reasons of scheduling efficiency, PET transmission scans are usually acquired 30 to 60 minutes after injection of FDG. When conventional PET transmission scans are taken postinjection, the photons from the radioisotope decay are collected along with the transmission photons, effectively contaminating the transmission scan. Because of the overwhelming flux from CT scanners, the photons from the decay do not affect the CT image. Fig. 5 summarizes these factors. Consequently, all PET/CT scanners have the capability of performing CT-based attenuation correction. CT transmission images, however, can result in biased PET attenuation correction factors. The following discussion addresses the cause of and some solutions for this bias.

Causes of CT-based attenuation correction bias

To correct accurately for the attenuation of 511-keV PET photons, one needs to have knowledge of the attenuation coefficient for 511-keV photons along each line of response of the PET scanner. Unfortunately, CT transmission images use photons in the range of 30 to 130 keV, resulting in incorrect estimates of the attenuation of 511-keV photons [32].

Attenuation coefficients are dependent on the photon energy and the type of material. In diagnostic imaging, the attenuation of photons is dominated by Compton scattering and photoelectric absorption interactions. Fig. 6 plots the total linear attenuation coefficients for muscle and bone along with their contributing photoelectric and Compton scatter components. Note that for energies below 50 keV, photoelectric absorption dominates and for higher energies in this range, Compton scatter dominates.

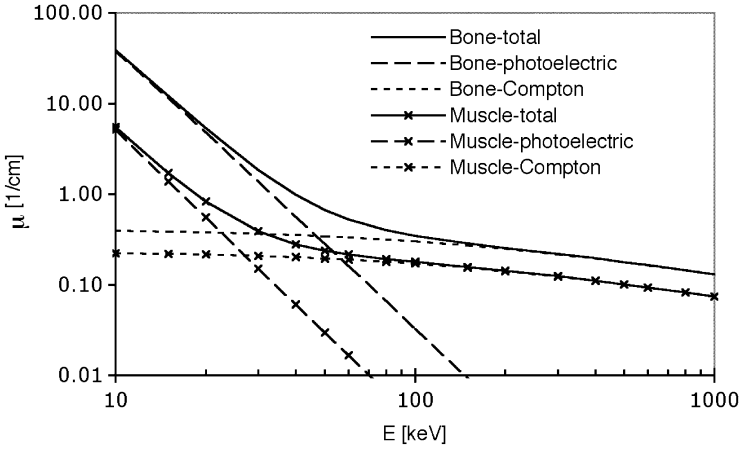

Fig. 6. Linear attenuation coefficients for bone and muscle tissue in the range of 10 to 1000 keV. Photoelectric absorption is the main contributor to the attenuation of photons at lower energies, whereas Compton scattering dominates at higher energies.

Another way to study the attenuation for a given material is to remove the dependence on material density ρ, leaving only a dependence on material atomic information and photon energy. This new term μ/ρ, the mass attenuation coefficient, appears in Fig. 7 for several biologic materials. In the region where Compton scattering dominates, the mass attenuation coefficients for all of the materials converge. An x-ray source emits photons with energies in the range of 30 to 130 keV where photoelectric absorption dominates; PET imaging occurs at 511 keV where Compton scattering dominates. Fig. 7 in relation to Fig. 6 shows that the 511-keV photon travel distance is dependent on the density of the material and only slightly dependent on the composition of the material. Attenuation of 30- to 130-keV photons, however, is dependent on the atomic composition of the material and density. That is, bone and adipose tissue attenuate photons very differently at 30 keV, but not at 511 keV. Fig. 7 reveals that there is not a simple linear rela-

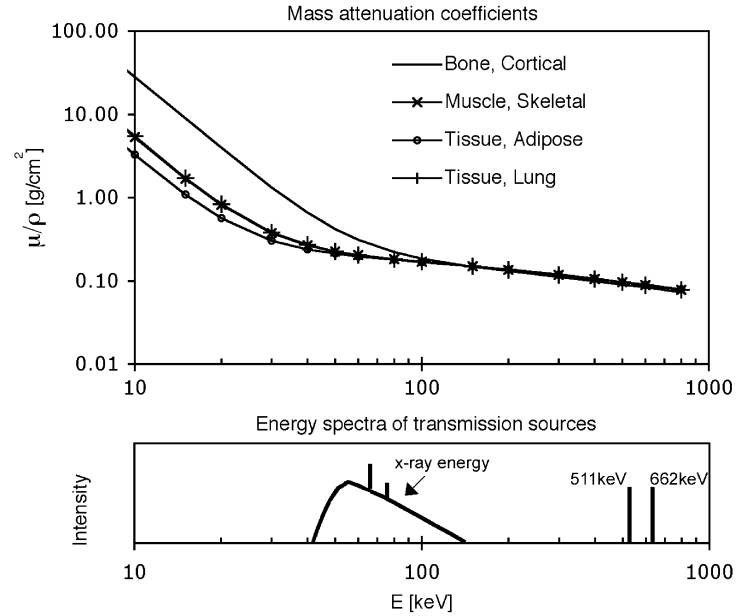

Fig. 7. Total mass attenuation coefficients for several biologic materials along with the spectral distribution for photons in x-ray and PET transmission sources.

tionship between x-ray attenuation values and PET attenuation values for all materials. Using a single scaling term to convert linear attenuation coefficients from CT energies to PET energies results in bias in the estimated attenuation image.

Even if one could differentiate the materials from each other and use a unique scaling term for each material, there is still some error because of the polyenergetic spectra of the x-ray source. In PET imaging, positrons annihilate causing the emission of two photons precisely at 511 keV with intensity I_0. The intensity, I, of these monoenergetic photons as they travel a distance t through matter along line t' follows the attenuation law

$$I(t) = I_0 \exp\left(- \int_0^t \mu(t', E = 511\text{keV}) dt' \right) \quad (1)$$

In contrast, an x-ray tube produces photons with wide spectra of energies (see Fig. 7). The intensity, I, of this polyenergetic photon beam as it travels distance t along a line is essentially the sum of the intensities of the photons at each energy, E, represented in the energy-weighted integral

$$\begin{aligned} I(t) &= \int_0^{E_{\max}} I(E) dE \\ &= \int_0^{E_{\max}} I_0(E) \exp\left(- \int_0^t \mu(t', E) dt' \right) dE \end{aligned} \quad (2)$$

Photoelectric absorption is dominant for lower energies causing a preferential attenuation of lower-energy photons. This forces the original energy spectrum to shift to higher energies resulting in the well-known beam-hardening effect. All commercial CT systems correct for beam-hardening during image reconstruction.

Even with beam-hardening corrections, there is no simple calibration to return to the true linear attenuation coefficients. CT images are represented in Hounsfield units (HU),

$$H(x,y) = 1000 \left(\frac{\hat{\mu}(x,y)}{\hat{\mu}_{\text{water}}} - 1 \right) \quad (3)$$

where μ (x,y) is the CT scanner's measured attenuation value at coordinate (x,y). This scale forces all water in the image have the value $H = 0$ and other materials to be relative to water. The conversion of CT HUs to linear attenuation coefficients is scanner-specific and even related to the path the photons had to travel. To get a sense of this conversion, Fig. 8 plots the measured HU of a few common tissues for a CT scanner with a tube voltage of 120 kV (peak) [36]. The fact that CT images must be represented with this relative scale without a direct conversion to linear attenuation coefficients further confounds the conversion of a CT attenuation image into a monoenergetic PET attenuation image.

Determining PET attenuation correction factors from CT

There are two common methods for converting CT image values to a 511-keV attenuation map. Simulation studies have shown that linear scaling from CT energies to other energies works well for materials with low atomic numbers (Z) [37]. Fig. 7 reinforces these findings because the soft tissues have very similar curves. High-Z materials, such as bone, do not scale the same as the soft tissues. This is the basis of using linear relationships to define the scaling factors of different tissue regions.

The bilinear conversion method uses a linear relationship with one slope for soft regions (air-water mixtures) and another slope for bone regions (water–bone mixtures) [38–40]. CT numbers in the range of $-1000 < H < 0$ are considered to represent regions with a mixture of air and soft tissue; CT numbers $H > 0$ represent regions with mixture of soft tissue and bone.

Similarly, the hybrid conversion method uses two linear relationships for regions considered either soft tissue or bone. For this method, the air-water regions are defined as $-1000 < H < 300$ and the air-bone mixture regions as $H > 300$ [41]. For the air-bone mixture regions, the linear relationship changes its y-intercept (not slope).

Fig. 8 displays the scaling relationship between CT numbers and the linear attenuation coefficients at 511-keV PET for the bilinear and hybrid methods. Note the correlation between the measured CT number values and the conversion methods. These conversion methods have been shown to provide attenuation corrections comparable with Ge-68 and Cs-137 transmission scans [42,43] for biologic materials.

Additional challenges for CT-based attenuation correction

As discussed in the image display section, spatial mismatch between the CT and PET scan can occur. Any form of patient movement and respiratory motion leads to erroneous attenuation correction factors resulting in degraded emission images [29,44]. CT

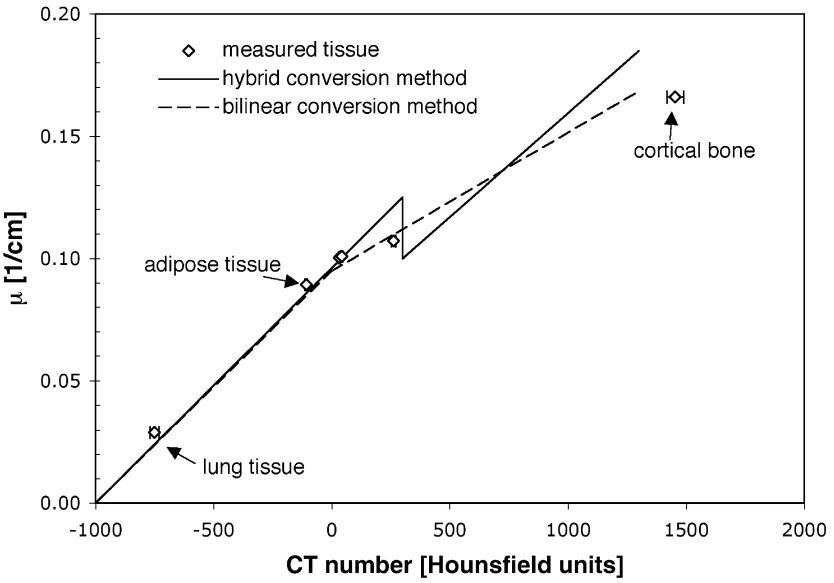

Fig. 8. A 511-keV linear attenuation coefficient, μ, of several biologic materials as a function of CT number. CT numbers were measured from a CT scanner with a tube voltage of 120 kV (peak) [34]. The hybrid and bilinear conversion methods translate CT attenuation numbers to PET 511-keV attenuation values.

scans often acquire a peak inspiration, whereas PET scans collect an averaged respiratory cycle. Fig. 9 shows the effects of respiratory motion in an image. Fig. 9C presents a CT taken during normal breathing with a liver artifact and Fig. 9D shows how this error appears in the attenuation-corrected PET image. In contrast, the CT in Fig. 9A, taken during a breathhold at normal expiration, has no errors and consequently the attenuation-corrected PET image (Fig. 9B) has no errors.

Qi et al [45] studied how the errors from respiratory mismatch propagate into the PET image through the attenuation correction. Fig. 10 shows the root mean square error of emission images from their true values when attenuation-correction factors are obtained at different points in the respiratory cycle. These results show that in some cases the least error occurs when the CT scan is taken at the middle of a breath. This partial expiration CT may, however, have reduced diagnostic quality. In the future, respiratory gated emission scans may offer another solution to alleviate these errors [46].

CT contrast agents further complicate the conversion of CT numbers to linear attenuation coefficients at 511 keV [47,48]. Contrast (caused by its atomic composition) strongly attenuates 30- to 140-keV x-ray photons by photoelectric absorption, leading to the desired enhanced regions in the CT image. Compton scattering dominates 511 keV annihilation photon attenuation, however, and mass attenuation is only weakly dependent on atomic composition. For instance, a contrast region in the CT image may have a CT number higher than bone ($H > 1000$), but 511-keV PET photons experience only the same attenuation as water ($H = 0$). Fig. 11 plots the mass attenuation coefficient versus energy for biologic material and the common intravenous contrast agent, iodine. The x-ray energy spectra and PET energy is overlaid on this graph to highlight the discrepancy between the attenuation values. In essence, the scale factor that predicts the attenuation at 511 keV for bone or soft tissue overestimates the attenuation at 511 keV for contrast agents. This error results in inaccurate uptake values in the emission scan.

Although initial studies indicate that these contrast errors may not be significant for diagnosis in a variety of cases [49], they afflict longitudinal studies where quantitation is important. Moreover, focal accumulation can occur, for example, in the case of oral contrast caused by delay in intestinal passage and in the case of intravenous contrast caused by bolus injections. These focal accumulations can result in strong artifacts in the attenuation-corrected PET image. One specific solution for oral contrast is to use a negative contrast agent (to alleviate the scaling

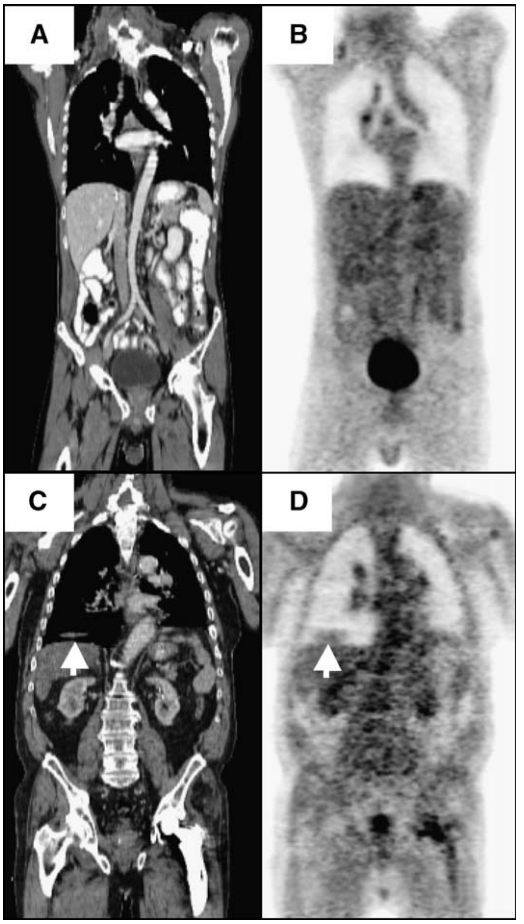

Fig. 9. Effect of respiratory motion in CT propagates into the emission image through the attenuation correction. (*A*) CT image using breathhold during thorax scan. (*B*) PET image using attenuation correction factors from Fig. 9A. (*C*) CT image of different patient during normal breathing. (*D*) PET image using attenuation correction factors from Fig. 9C clearly shows an artifact above liver (*arrow*) caused by the liver dome being mirrored at the right lung base. (Courtesy of Thomas Beyer, PhD, University of Essen, Essen, Germany.)

discrepancy) with a better bowel distention (to reduce accumulation) [50]. Fig. 12 presents an example of intravenous contrast agents causing artifacts in the attenuation-corrected PET image. Fig. 12C is the difference image between emission images using attenuation-correction factors from contrast CT and noncontrast CT. The greatest errors are caused by the focal accumulation of contrast along the aorta and are caused by respiratory motion mismatch. Diffuse contrast collection, such as in the kidneys, causes little to no error in the emission image (Fig. 12C, arrow 3). A general solution for these errors is to use segmentation methods to define contrast-enhanced regions and then use appropriate scaling terms in these regions [51,52].

Metallic objects, such as prostheses [53] and dental implants [54], also complicate the use of CT-based attenuation correction. CT transmission scans are more prone to produce strong artifacts around metallic objects than the common PET transmission scans. These artifacts propagate through the attenuation correction into the emission image. Lower-dose CT can help reduce some of these artifacts. Currently, there are no clear methods for overcoming this challenge.

Dual-energy x-ray imaging provides a more accurate solution for getting 511-keV attenuation information. Collecting two (or more) scans with x-ray beams at different energies allows one to decouple the photoelectric absorption and Compton scattering components from the total linear attenuation coefficients [55]. These individual components can then be scaled separately to any energy, such as 511 keV for PET, and added to obtain the total attenuation coefficient. This method has some drawbacks because of the need for a second CT scan requiring more dosage for the patient and more time. A potential solution is to use a single CT scan with alternating x-ray energies on alternating slices [56] or to use a second very-low-dose CT scan. Both the dual-energy decoupling and a low-dose CT scan

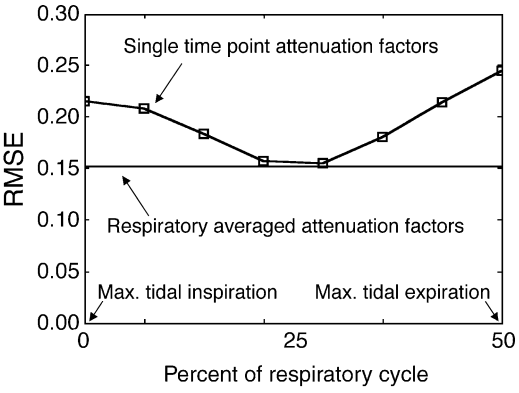

Fig. 10. Root mean square error (RMSE) of simulated emission images reconstructed with attenuation correction factors collected at different times in the respiratory cycle. The error calculated from a lesion in the dome of the liver. (Courtesy of Jinyi Qi, PhD, University of California at Davis, Davis, CA.)

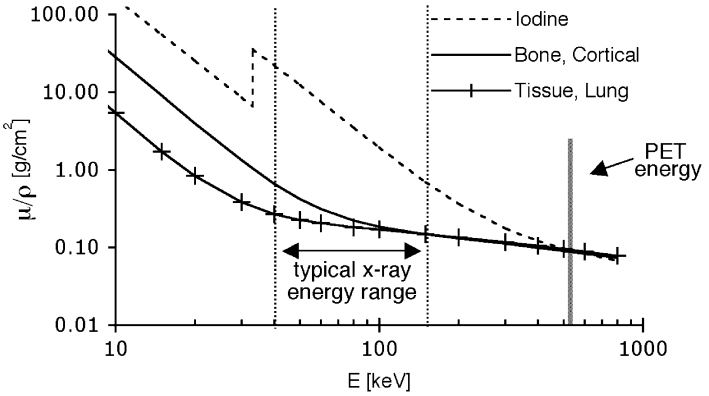

Fig. 11. Figure illustrating that mass attenuation coefficient of iodine is appreciably different from biologic tissue at CT energies, whereas similar at PET 511-keV energy.

contribute noise that is unacceptable for a diagnostic CT image. For PET attenuation correction, however, the image quality is likely acceptable.

CT truncation and beam-hardening artifacts also lead to errors in the attenuation-corrected image. Current helical CT offers a transverse field of view of 50 cm, about 20 cm less than the PET imaging field of view. This poses a problem considering that most patients are imaged arms down during PET scans for patient comfort. Truncation of the CT image results in missing information for certain lines of response in the emission image. The wrong attenuation correction factors are further compounded with any beam-hardening artifacts. Methods have been developed to reduce these errors and estimate the missing information [57,58]. Fig. 13 provides a simulated example of the artifacts from using truncated CT for attenuation correction.

A general approach to help alleviate all of these CT attenuation-correction challenges is to adopt appropriate acquisition protocols [59]. For instance, accepting an intentional breathing pattern can help reduce respiratory motion artifacts. Likewise, the required CT quality governs many of the parameters found here including contrast agents, respiratory patterns, patient positioning, and likelihood of truncation.

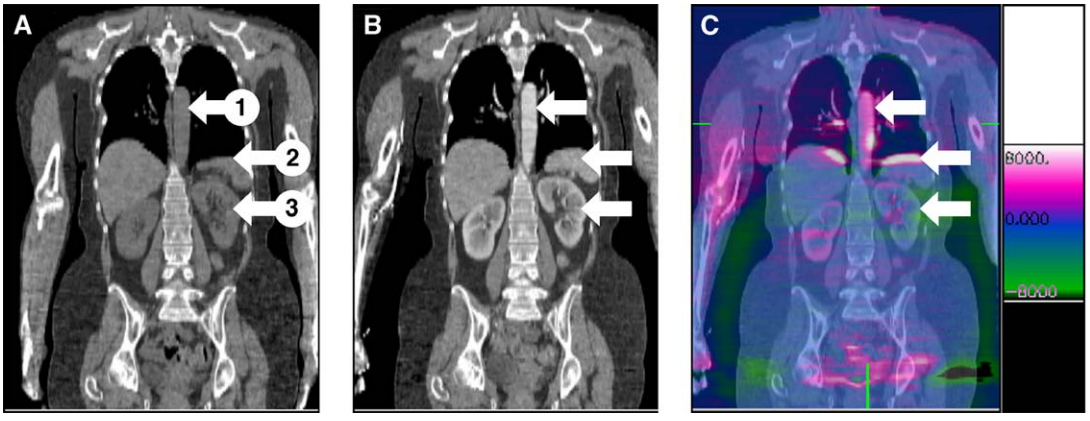

Fig. 12. (*A*) Nonenhanced CT image. (*B*) Intravenous contrast-enhanced CT image through same coronal plane. (*C*) Difference image obtained by subtracting the emission scans after attenuation correction by A or B, respectively (the difference data are superimposed on Fig. 12B for anatomic localization of errors). Difference image shows positive differences in white, zero difference in blue, and negative differences in green shades. The white region along the aorta (*arrow 1*) shows incorrectly elevated uptake values caused by focal contrast accumulation. Arrow 2 highlights the error caused by respiratory motion. Arrow 3 illustrates an example where contrast agent accumulation does not significantly alter PET image appearance, although there may be quantitative changes.

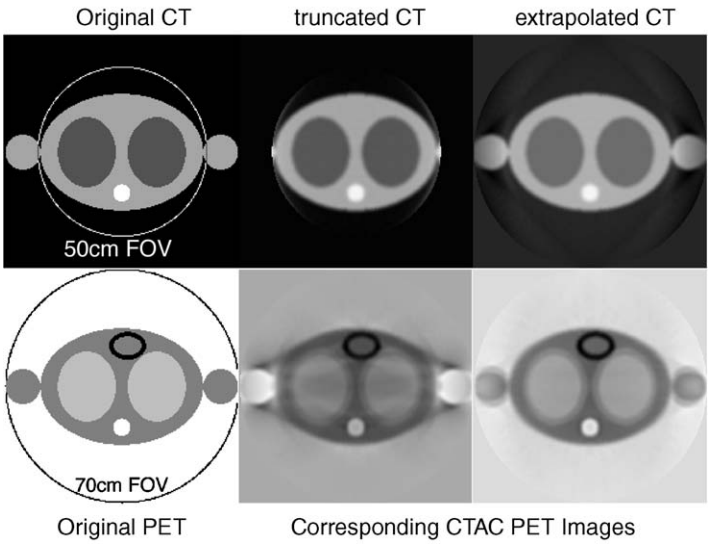

Fig. 13. Simulation example of truncation errors in attenuation-corrected PET images. Top row shows gray scale CT images; bottom row shows associated inverse gray scale PET emission images. Truncating CT data in the second column causes significant artifacts in the PET image. Simple extrapolation of CT data as done in the third column helps reduce such artifacts. FOV, field of view.

Several factors complicate the use of CT for PET attenuation correction. It should be stressed that the benefits of CT attenuation correction, namely its noise-free quality and speed, significantly outweigh these complications and have motivated the trend of vendors to offer only CT-based attenuation correction. The clinician needs to be aware of the possible causes of bias in the attenuation correction and should carefully inspect all three images (CT and PET emission with and without attenuation correction) when appropriate.

Present and future summary

Even though the clinical efficacy of PET/CT has not been proved, this technology has become extremely popular in the last 4 years, with approximately 400 installed scanners worldwide. PET/CT offers a simple hardware solution for viewing anatomic and functional images and a significant reduction in emission imaging time because of the use of CT-based attenuation correction. These same benefits also pose technical challenges. Specifically, the final image alignment is still prone to minor error and the translation of CT values to PET energies for attenuation correction suffers from several complications.

The future of PET/CT awaits the results from clinical studies evaluating this technology for tasks including diagnosis, serial follow-up, and radiation treatment planning. In the meantime, PET/CT systems continue to evolve to include improved software and hardware features. New techniques are being explored for CT-guided PET image reconstruction ultimately to improve detection or quantitation [60–62]. Methods for gated PET offer promising solutions for respiratory motion artifacts [46]. This new technology coupled with the dynamic benefits of multislice CT may provide valuable information for coronary disease [63]. In general, the overall progression of PET/CT scanners is to supply better PET performance through faster, smaller detectors and improved electronics. The CT component trend is to offer more slices providing faster scans and catering to cardiology applications. There is also a need for less expensive hardware perhaps through a truly integrated system with shared gantries, electronics, and processors. At the current rate of progress, PET/CT is poised to become an effective, accessible, and widely used imaging modality.

Acknowledgments

The authors thank Dr. Jinyi Qi of the University of California at Davis, Dr. Thomas Beyer of the University of Essen, and Dr. Jacqueline Brunetti and Allan Caggiano of Holy Name Hospital for sharing

their results and data. They also thank David Faul and Richard Powers of CPS, Steven Kohlmyer and Michael O'Keefe of General Electric Healthcare, and Mark Stohr of Philips Medical Systems for their assistance.

References

[1] Weber WA, Avril N, Schwaiger M. Relevance of positron emission tomography (PET) in oncology. Strahlenther Onkol 1999;175:356–73.
[2] Bomanji JB, Costa DC, Ell PJ. Clinical role of positron emission tomography in oncology. Lancet Oncol 2001;2:157–64.
[3] Hustinx R, Benard F, Alavi A. Whole-body FDG-PET imaging in the management of patients with cancer. Semin Nucl Med 2002;32:35–46.
[4] Delbeke D, Martin WH. Positron emission tomography imaging in oncology. Radiol Clin North Am 2001; 39:883–917.
[5] Maes F, Collignon A, Vandermeulen D, Marchal G, Suetens P. Multimodality image registration by maximization of mutual information. IEEE Trans Med Imaging 1997;16:187–98.
[6] Slomka PJ. Software approach to merging molecular with anatomic information. J Nucl Med 2004;45: 36S–45S.
[7] Mattes D, Haynor DR, Vesselle H, Lewellen TK, Eubank W. PET-CT image registration in the chest using free-form deformations. IEEE Trans Med Imaging 2003;22:120–34.
[8] West J, Fitzpatrick JM, Wang MY, Dawant BM, Maurer Jr CR, Kessler RM, et al. Comparison and evaluation of retrospective intermodality brain image registration techniques. J Comput Assist Tomogr 1997; 21:554–66.
[9] West J, Fitzpatrick JM, Wang MY, Dawant BM, Maurer Jr CR, Kessler RM, et al. Retrospective intermodality registration techniques for images of the head: surface-based versus volume-based. IEEE Trans Med Imaging 1999;18:144–50.
[10] Lang TF, Hasegawa BH, Liew SC, Brown JK, Blankespoor SC, Reilly SM, et al. Description of a prototype emission-transmission computed tomography imaging system. J Nucl Med 1992;33:1881–7.
[11] Beyer T, Townsend D, Brun T, Kinahan P, Charron M, Roddy R, et al. A combined PET-CT scanner for clinical oncology. J Nucl Med 2000;41:1369–79.
[12] Schoder H, Yeung HW, Gonen M, Kraus D, Larson SM. Head and neck cancer: clinical usefulness and accuracy of PET-CT image fusion. Radiology 2004; 231:65–72.
[13] Goerres GW, von Schulthess GK, Steinert HC. Why most PET of lung and head-and-neck cancer will be PET-CT. J Nucl Med 2004;45(Suppl 1):66S–71S.
[14] Fukui MB, Blodgett TM, Meltzer CC. PET-CT imaging in recurrent head and neck cancer. Semin Ultrasound CT MR 2003;24:157–63.
[15] Zimmer LA, McCook B, Meltzer C, Fukui M, Bascom D, Snyderman C, et al. Combined positron emission tomography/computed tomography imaging of recurrent thyroid cancer. Otolaryngol Head Neck Surg 2003;128:178–84.
[16] Lardinois D, Weder W, Hany TF, Kamel EM, Korom S, Seifert B, et al. Staging of non-small-cell lung cancer with integrated positron-emission tomography and computed tomography. N Engl J Med 2003;348: 2500–7.
[17] Schoder H, Larson SM, Yeung HW. PET-CT in oncology: integration into clinical management of lymphoma, melanoma, and gastrointestinal malignancies. J Nucl Med 2004;45(Suppl 1):72S–81S.
[18] Antoch G, Kanja J, Bauer S, Kuehl H, Renzing-Koehler K, Schuette J, et al. Comparison of PET, CT, and dual-modality PET-CT imaging for monitoring of imatinib (STI571) therapy in patients with gastrointestinal stromal tumors. J Nucl Med 2004;45:357–65.
[19] Wahl RL. Why nearly all PET of abdominal and pelvic cancers will be performed as PET-CT. J Nucl Med 2004;45(Suppl 1):82S–95S.
[20] Pannu HK, Bristow RE, Cohade C, Fishman EK, Wahl RL. PET-CT in recurrent ovarian cancer: initial observations. Radiographics 2004;24:209–23.
[21] Makhija S, Howden N, Edwards R, Kelley J, Townsend DW, Meltzer CC. Positron emission tomography/computed tomography imaging for the detection of recurrent ovarian and fallopian tube carcinoma: a retrospective review. Gynecol Oncol 2002;85:53–8.
[22] Metser U, Lerman H, Blank A, Lievshitz G, Bokstein F, Even-Sapir E. Malignant involvement of the spine: assessment by 18F-FDG-PET-CT. J Nucl Med 2004; 45:279–84.
[23] Czernin J. Summary of selected PET-CT abstracts from the 2003 Society of Nuclear Medicine Annual Meeting. J Nucl Med 2004;45:102S–3S.
[24] Schwartz DL, Ford E, Meyer J, Rajendran J, Lewellen B, Yueh B, et al. Co-registered FDG-PET-CT imaging for staging and IMRT treatment planning for squamous cell carcinoma of the head and neck. Int J Radiat Oncol Biol Phys 2003;57:S156–7.
[25] Esthappan J, Mutic S, Malyapa RS, Grigsby PW, Zoberi I, Dehdashti F, et al. Treatment planning guidelines regarding the use of CT/PET-guided IMRT for cervical carcinoma with positive para-aortic lymph nodes. Int J Radiat Oncol Biol Phys 2004;58: 1289–97.
[26] Ciernik IF, Dizendorf E, Baumert BG, Reiner B, Burger C, Davis JB, et al. Radiation treatment planning with an integrated positron emission and computer tomography (PET-CT): a feasibility study. Int J Radiat Oncol Biol Phys 2003;57:853–63.
[27] Rehm K, Strother S, Anderson J, Schaper K, Rottenberg D. Display of merged multimodality brain images using interleaved pixels with independent color scales. J Nucl Med 1994;35:1815–21.

[28] Stearns C, Miesbauer D, Culp R. Measuring gantry-gantry and gantry-table alignment in PET-CT. In: IEEE Nuclear Science Symposium and Medical Imaging Conference Record, 2003.
[29] Beyer T, Antoch G, Blodgett T, Freudenberg LF, Akhurst T, Mueller S. Dual-modality PET-CT imaging: the effect of ACF-artifact, respiratory motion on combined image quality in clinical oncology. Eur J Nucl Med 2003;30:588–96.
[30] Nakamoto Y, Tatsumi M, Cohade C, Osman M, Marshall LT, Wahl RL. Accuracy of image fusion of normal upper abdominal organs visualized with PET-CT. Eur J Nucl Med 2003;30:597–602.
[31] Goerres GW, Kamel E, Heidelberg T-NH, Schwitter MR, Burger C, Schulthess GKv. PET-CT image co-registration in the thorax: influence of respiration. Eur J Nucl Med 2002;29:351–60.
[32] Kinahan PE, Hasegawa BH, Beyer T. X-ray-based attenuation correction for positron emission tomography/computed tomography scanners. Semin Nucl Med 2003;33:166–79.
[33] Wahl RL. To AC or not to AC: that is the question. J Nucl Med 1999;40:2025–8.
[34] Bai C, Kinahan PE, Brasse D, Comtat C, Townsend DW, Meltzer CC, et al. An analytic study of the effects of attenuation on tumor detection in whole-body PET oncology imaging. J Nucl Med 2003;44:1855–61.
[35] Beyer T, Kinahan PE, Townsend DW. Optimization of transmission and emission scan duration in 3D whole-body PET. IEEE Trans Nucl Sci 1997;44:2400–7.
[36] Schneider W, Bortfeld T, Schlegel W. Correlation between CT numbers and tissue parameters needed for Monte Carlo simulations of clinical dose distributions. Phys Med Biol 2000;45:459–78.
[37] LaCroix KJ, Tsui BMW, Hasegawa BH, Brown JK. Investigation of the use of x-ray CT images for attenuation compensation in SPECT. IEEE Trans Nucl Sci 1994;41:2793–9.
[38] Blankespoor SC, Xu X, Kaiki K, Brown JK, Tang HR, Cann CE, et al. Attenuation correction of SPECT using x-ray CT on an emission-transmission CT system: myocardial perfusion assessment. IEEE Trans Nucl Sci 1996;43:2263–74.
[39] Burger C, Goerres G, Schoenes S, Buck A, Lonn AH, Von Schulthess GK. PET attenuation coefficients from CT images: experimental evaluation of the transformation of CT into PET 511-keV attenuation coefficients. Eur J Nucl Med Mol Imaging 2002;29:922–7.
[40] Bai C, Shao L, Da Silva AJ, Zhao Z. A generalized model for the conversion from CT numbers to linear attenuation coefficients. IEEE Trans Nucl Sci 2003;50:1510–5.
[41] Kinahan PE, Townsend DW, Beyer T, Sashin D. Attenuation correction for a combined 3D PET-CT scanner. Med Phys 1998;25:2046–53.
[42] Nakamoto Y, Osman M, Cohade C, Marshall LT, Links JM, Kohlmyer S, et al. PET-CT: comparison of quantitative tracer uptake between germanium and CT transmission attenuation-corrected images. J Nucl Med 2002;43:1137–43.
[43] Kamel E, Hany TF, Burger C, Treyer V, Lonn AH, von Schulthess GK, et al. CT vs 68Ge attenuation correction in a combined PET-CT system: evaluation of the effect of lowering the CT tube current. Eur J Nucl Med Mol Imaging 2002;29:346–50.
[44] Goerres GW, Burger C, Kamel E, Seifert B, Kaim AH, Buck A, et al. Respiration-induced attenuation artifact at PET-CT: technical considerations. Radiology 2003;226:906–10.
[45] Qi J, Huesman RH, Reutter BW. Comparison of different CT-based attenuation correction schemes for PET with respiratory motion [abstract]. J Nucl Med 2003;44:P121.
[46] Boucher L, Rodrigue S, Lecomte R, Benard F. Respiratory gating for 3-dimensional PET of the thorax: feasibility and initial results. J Nucl Med 2004;45:214–9.
[47] Cohade C, Osman M, Nakamoto Y, Marshall LT, Links JM, Fishman EK, et al. Initial experience with oral contrast in PET-CT: phantom and clinical studies. J Nucl Med 2003;44:412–6.
[48] Antoch G, Freudenberg LS, Egelhof T, Stattaus J, Jentzen W, Debatin JF, et al. Focal tracer uptake: a potential artifact in contrast-enhanced dual-modality PET-CT scans. J Nucl Med 2002;43:1339–42.
[49] Dizendorf E, Hany TF, Buck A, von Schulthess GK, Burger C. Cause and magnitude of the error induced by oral CT contrast agent in CT-based attenuation correction of PET emission studies. J Nucl Med 2003;44:732–8.
[50] Antoch G, Kuehl H, Kanja J, Lauenstein TC, Schneemann H, Hauth E, et al. Dual-modality PET-CT scanning with negative oral contrast agent to avoid artifacts: introduction and evaluation. Radiology 2004;230:879–85.
[51] Nehmeh SA, Erdi YE, Kalaigian H, Kolbert KS, Pan T, Yeung H, et al. Correction for oral contrast artifacts in CT attenuation-corrected PET images obtained by combined PET-CT. J Nucl Med 2003;44:1940–4.
[52] Carney J, Beyer T, Brasse D, Yap JT, Townsend DW. CT-based attenuation correction for PET-CT scanners in the presence of contrast agent. Nuclear Science Symposium Conference Record, 2002 IEEE, 2002;3:1443–6.
[53] Goerres GW, Ziegler SI, Burger C, Berthold T, von Schulthess GK, Buck A. Artifacts at PET and PET-CT caused by metallic hip prosthetic material. Radiology 2003;226:577–84.
[54] Kamel EM, Burger C, Buck A, von Schulthess GK, Goerres GW. Impact of metallic dental implants on CT-based attenuation correction in a combined PET-CT scanner. Eur Radiol 2003;13:724–8.
[55] Alvarez RE, Macovski A. Energy-selective reconstructions in x-ray computerized tomography. Phys Med Biol 1976;21:733–44.

[56] Guy MJ, Castellano-Smith IA, Flower MA, Flux GD, Ott RJ, Visvikis D. DETECT-dual energy transmission estimation CT-for improved attenuation correction in SPECT and PET. IEEE Trans Nucl Sci 1998;45: 1261–7.
[57] Lonn AH, Hsieh J, Stearns C, Chao EH, Grekowicz B. Evaluation of extension of the CT attenuation map in PET-CT [abstract]. J Nucl Med 2003;44:P123.
[58] Carney J, Townsend D, Kinahan P, Beyer T, Kachelriess M, Kalender WA, et al. CT-based attenuation correction: the effects of imaging with the arms in the field of view [abstract]. J Nucl Med 2001;42: 56P–7P.
[59] Beyer T, Antoch G, Muller S, Egelhof T, Freudenberg LS, Debatin J, et al. Acquisition protocol considerations for combined PET-CT imaging. J Nucl Med 2004;45:25S–35S.
[60] Politte DG, Snyder DL. Image reconstruction for position-emission tomography when anatomical boundaries are known. In: Nuclear Science Symposium and Medical Imaging Conference, 1991. Conference Record of the 1991 IEEE, 1991;3:1926.
[61] Gindi G, Lee M, Rangarajan A, Zubal IG. Bayesian reconstruction of functional images using anatomical information as priors. IEEE Trans Med Imaging 1993;12:670–80.
[62] Comtat C, Kinahan PE, Fessler JA, Beyer T, Townsend DW, Defrise M, et al. Clinically feasible reconstruction of 3D whole-body PET-CT data using blurred anatomical labels. Phys Med Biol 2002;47:1–20.
[63] Slart RHJA, Bax JJ, de Jong RM, de Boer J, Lamb HJ, Mook PH, et al. Comparison of gated PET with MRI for evaluation of left ventricular function in patients with coronary artery disease. J Nucl Med 2004;45: 176–82.